PHYSICAL REVIEW C VOLUME 52, NUMBER 6 DECEMBER 1995

Muon-induced neutron and pion production in an organic liquid scintillator at a shallow depth

R. Hertenberger* and M. Chen†
Norman Bridge Laboratory of Physics, California Institute of Technology, Pasadena, California 91125

B. L. Dougherty‡
Department of Physics, Stanford University, Stanford, California 94305

(Received 4 May 1995)

The production of fast neutrons and pions by inelastic interactions of cosmic-ray muons in an organic liquid scintillator has been investigated. A detector filled with 190 liters of a 0.09% gadolinium-loaded liquid scintillator was installed in the Stanford Underground Facility, at an underground depth of approximately 20 meters water equivalent. The detector served as the target material for hadron production. Our measurements find a single-neutron production yield of $(4.3\pm0.3\pm0.8)\times10^{-5}$ neutrons per muon g/cm^2 and a double-neutron production yield of $(1.6\pm0.2\pm0.5)\times10^{-5}$ double neutrons per muon g/cm^2. We measured a π^+ production yield of $(3.5\pm0.2\pm0.7)\times10^{-6}$ pions per muon g/cm^2. Nearly all the π^+ produced were accompanied by neutrons. These yields were dependent on the energy threshold of the muon trigger, revealing an enhancement associated with hadronic showers initiated by muons. The production yield due to nonshowering muons was lower: 2×10^{-5} neutrons per muon g/cm^2, with a single-to-double neutron multiplicity ratio of roughly 4:1. The nonshowering muon π^+ production probability was 2.5×10^{-6} pions per muon g/cm^2, with about half of these nonshowering π^+ events accompanied by neutrons.

PACS number(s): 29.40.Mc, 13.10.+q, 13.60.−r, 98.70.Sa

I. INTRODUCTION

The San Onofre reactor antineutrino detector [1] will be the first large volume (12-ton) neutrino experiment to operate at a shallow underground depth of only 25 m water equivalent (mwe). At this depth, the intense muon flux poses a background challenge through the muon-induced production of hadrons and radioactivity, which appear as unvetoable delayed events in the detector. In particular, the correlated production of multiple neutrons by an inelastic muon interaction is a background that is able to mimic the inverse beta decay signal used for the detection of the reactor $\bar{\nu}_e$. In order to further our understanding of these backgrounds, a new measurement of muon spallation products was initiated. This measurement is also relevant to experiments that search for dark-matter-induced nuclear recoils in cryogenic detectors [2]. These experiments are starting now with measurements at shallow depth underground locations, where the nuclear recoils from muon-generated fast neutrons become the most significant background to the dark-matter signal. A better understanding of the production of neutrons and pions at shallow depth is necessary.

The goal of this study was to determine the production rate of single and double neutrons in an organic liquid scintillator by inelastic muon interactions. Care has been taken to avoid contributions from muon capture. For deeper insight into the production of multiple neutrons, we also measured the production yield of pions. Additionally, we observed the production of neutrons accompanying these pions.

Negative pions provide a mechanism for subsequent multiple neutron production via their interaction with a pseudodeuteron in a ^{12}C nucleus: $\pi^- + d \rightarrow n + n$. In our measurement, this channel was only accessible by neutron detection and could not be distinguished from other neutron production mechanisms. We were, however, sensitive to the production of π^+ via the $\pi^+ \rightarrow \mu^+ \rightarrow e^+$ decay. This can provide information on the π^- component of neutron production (from the charge independency of the strong interaction). In the production of a π^+ by an electromagnetic interaction of a cosmic-ray muon on ^{12}C: $\mu^+ + {}^{12}\mathrm{C} \rightarrow \mu^+ + \pi^+ + {}^{12}\mathrm{B}^*$, an excited boron nucleus results, potentially emitting nucleons. Thus, it is also interesting to detect the neutrons associated with the π^+ events.

Our measurement involved detector materials relevant to the 12-ton neutrino oscillation experiment, namely, a Gd-loaded liquid scintillator, used simultaneously as the target material for neutron production and as the neutron detector itself. The underground measurement was performed in the Stanford Underground Facility. This laboratory is shielded by an approximately 20-mwe overburden, similar to that planned for the oscillation experiment. As we were interested in reliably measuring the double-neutron yield and other multihadronic channels, it was necessary to relinquish any passive shielding around the detector. The use of high Gd loading in the scintillator enabled the detection of neutrons within a short coincidence time and with an energy threshold above the background from natural radioactivity, minimizing the accidental background.

A. Experimental apparatus

With consideration for the low neutron yield from the muon spallation process and the moderation length of fast

---

*Present address: Sektion Physik, University of Munich, Am Coulombwall 1, D-85748 Garching, Germany.

†Present address: Physics Department, Princeton University, Princeton, NJ 08544.

‡Present address: Jet Propulsion Laboratory, 4800 Oak Grove Dr., Pasadena, CA 91109.

0556-2813/95/52(6)/3449(11)/$06.00

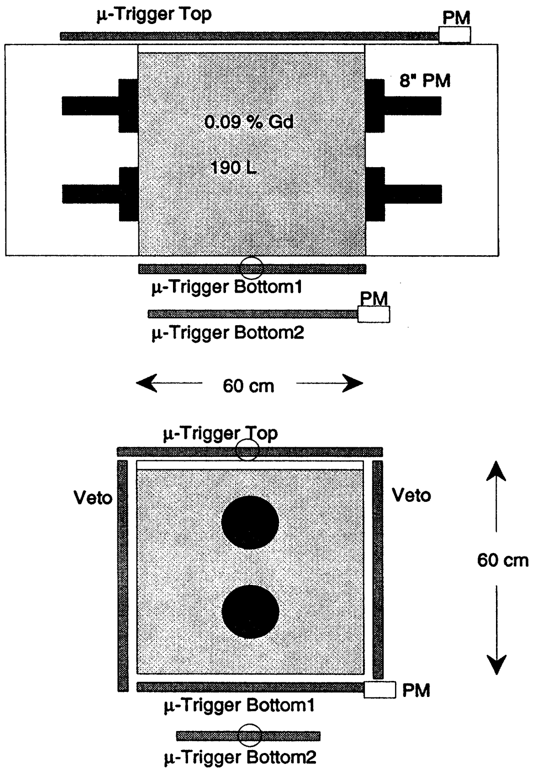

FIG. 1. The CUBE detector with muon veto counters. The top and the bottom veto paddles also served as trigger counters.

neutrons (≈50 cm), we designed an acrylic cubical vessel, of dimension (60 cm)^3. The cosmic-ray underground background experiment (CUBE) was filled with 190 l of Gd-loaded liquid scintillator (Fig. 1).

The 0.09% concentration of Gd was verified by neutron activation measurements, by inductively coupled plasma mass spectrometry (ICP-MS), and by the direct measurement of the 25-μs mean neutron capture time. The light yield of our scintillator was 55% relative to anthracene; its light attenuation length was determined in our vertical column spectrophotometer to be 6.8 m, at a wavelength of 440 nm.

Four 8-in-diam, Hamamatsu R1408 photomultipliers were mounted outside of the CUBE on two opposite sides, viewing the scintillation light. These hemispherical bulbs were coupled to the acrylic vessel walls using acrylic wedge-shaped adapters and reflective mirrors.

Surrounding the CUBE on the four sides that do not have photomultipliers attached to them were plastic scintillator muon veto counters. The top and bottom counters functioned as trigger and veto and the side counters as muon veto only. Figure 1 shows the arrangement of the veto counters around the main detector. The entire apparatus was placed on a 76-cm-high, square aluminum table, 60 × 60 cm^2. The placement of the detector, positioned in the middle of the underground facility and off the floor, reduced the probability for any neutron or pion, produced by muons in the walls of the tunnel, to reach the detector. In this way we attempted to measure neutron production in the liquid scintillator itself.

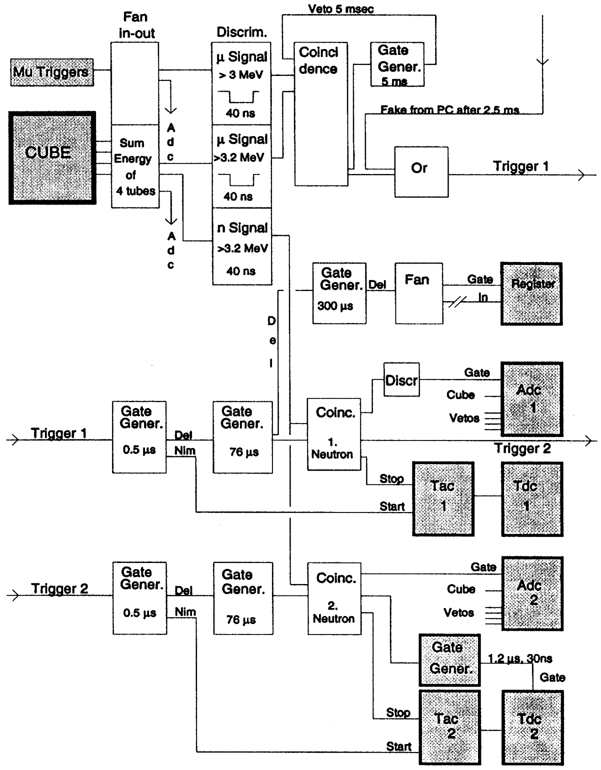

FIG. 2. Schematic of the CUBE electronics. The shaded items to the left were detector components; shaded items to the right were CAMAC modules; unshaded modules were implemented in NIM crates.

B. Experimental method and data acquisition

A schematic of the data acquisition and trigger electronics is presented in Fig. 2. The detector triggered on muons that had passed through it, in coincidence with scintillating paddles above and below the detector. Following a through-going muon trigger, we searched within 76 μs for the energetic signal of neutron capture on Gd (γ burst of about 8 MeV) or for the Michel positrons from $\pi^+(\mu^+)$ decay. The energy and time of up to two delayed signals could be recorded in two successive windows of 76 μs each, the second window commencing 0.5 μs after any first delayed count. Two analog-to-digital converters (ADC1 and ADC2) and two time-to-analog converters (TAC1 and TAC2) stored the energies and times of the first and second delayed signals, respectively. The nature of the delayed signals can be determined by their characteristic decay time: neutron signals have a mean capture time constant of 25 μs; the π^+ signals possess the 2.2-μs lifetime of the muon. The discriminator threshold for the delayed events of about 3.2 MeV was well enough above the natural radioactive background (2.6 MeV ^{208}Tl line) that we were able to operate our detector unshielded, without suffering from too large an accidental background.

The summed signals of the four photomultiplier tubes of the CUBE and the signals from the surrounding muon veto counters were fed into charge-integrating ADC's. When data from the CUBE were being recorded, the signals of the veto counters were also stored for off-line analysis.

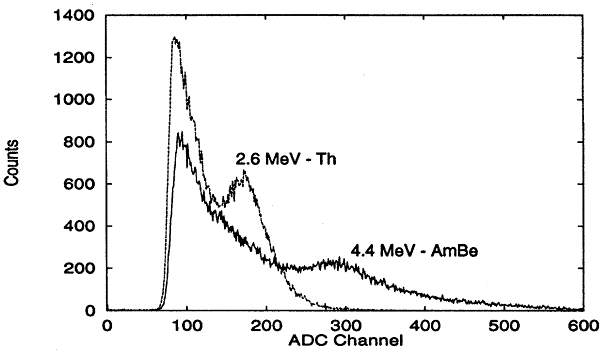

FIG. 3. Th and AmBe calibration spectra.

Quasisimultaneously to the signal, accidental background spectra were accumulated. Following a valid muon trigger, the data acquisition computer would initiate a false retriggering of the electronics, 2–3 ms after the true trigger. The purpose of this "false" trigger was to provide a contemporaneous measurement of the accidental background, which occurs by chance within the correct time window. This false trigger provides a reliable data set with equivalent statistics to be used for subtraction of the accidental background component.

C. Energy and time calibrations

The CUBE was calibrated with three energies, 0, 2.6 and 4.4 MeV. Figure 3 shows the calibration spectra taken with a Th source (γ at 2.6 MeV) and an AmBe neutron source, which also emits 4.4 MeV γ's. The energy calibratrion is linear over this range. The data acquisition threshold of 3.2 MeV lies at about channel 275, between the calibration points. Channel 670 corresponds to 8 MeV, the total energy of the γ burst released after the capture of a neutron on Gd. The spectrum taken with the AmBe source, which should contain these neutron capture events, ends somewhere near channel 700, in agreement. The TAC timing calibrations, performed with fixed start-stop intervals, were linear as well.

D. Neutron efficiency calibration and neutron capture time

The total neutron detection efficiency of the experiment can be separated into three components. First, there is the neutron capture efficiency — the likelihood for the muon-produced fast neutrons to thermalize and capture in the CUBE. Second, there is the requirement that the γ's sharing the 8-MeV total energy, following the neutron capture on Gd, are detected above the 3.2 MeV threshold. Finally, there is an efficiency term that is introduced by the analysis cuts — in particular, the selected time window for detection of the neutron capture signal.

The greatest systematic uncertainty in our measurement lies in estimating the neutron capture efficiency as the understanding of the energy spectrum of the neutrons from muon spallation is somewhat limited. According to Barton [3], the spectrum of neutrons from hadronic cascades falls off in energy as $\sim E_n^{-1/2}$ between 10 and 50 MeV, and the process of π^- capture by pseudodeuterons produces neutrons with a flat spectrum up to about 100 MeV. However, the intensities of these neutron production branches, including the excitation of the giant dipole resonance followed by neutron evaporation at low energies, are not well specified in any reference. A combined shape of

$$K\times(9.7E_n^{-1/2}+6.0e^{-E_n/10})$$

was used to approximate the spectrum. This spectrum, suggested by [4], was previously used in [5] to successfully model the spectrum of neutrons at shallow depth.

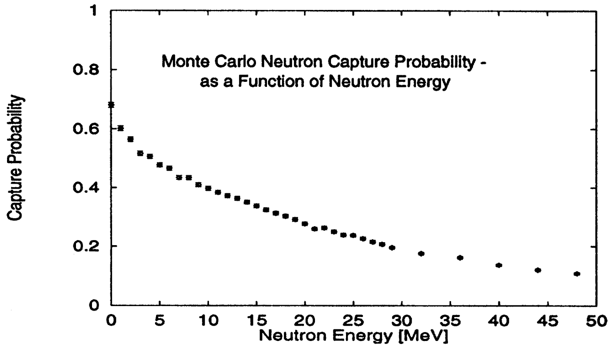

FIG. 4. Monte Carlo calculation of the neutron capture probability in the CUBE detector. Neutrons were produced homogeneously in the volume and it was required that the neutron be captured on Gd, within the detector.

A neutron Monte Carlo was employed to model the capture probability of fast spallation neutrons on Gd, within the volume of the CUBE detector. Figure 4 shows the estimated capture probabilities as a function of neutron energy for monoenergetic neutrons distributed uniformly throughout the detector volume. The folding of this efficiency curve with the spallation neutron energy spectrum results in an aggregate neutron capture probability of 37%. We accept an uncertainty in this calculation of 20%, coming from the inability to pin down the exact shape of the neutron energy spectrum.

The neutron transport code includes elastic scattering on H and C, the inelastic scattering cross sections on C and the neutron capture cross sections on H and Gd. Figure 5 presents the simulated neutron capture time in a 0.09% Gd-loaded liquid scintillator. The prediction is in agreement with the measured capture time of 25 μs and our observation of a neutron thermalization time of about 4 μs.

The γ portion of the efficiency was estimated using the EGS4 Monte Carlo code. The probabilities and energies for γ's in the cascade following neutron capture on ^{157}Gd were extracted from [6]. We estimate a γ detection probability of 38 ± 4%, above the 3.2 MeV threshold.

In the analysis, we select events based on energy, veto, and time information. The only significant term contributing to the detection efficiency comes from the time window of 9–76 μs. Within this interval, 78% of the neutron captures on Gd are detected, taking into account the 25-μs mean capture time and the neutron thermalization time of 4 μs. Thus, we arrive at a total neutron detection efficiency of 0.11 ± 0.02 for events that recorded a single neutron.

A measurement of the neutron detection efficiency was performed with an AmBe source. Here, a neutron trigger was

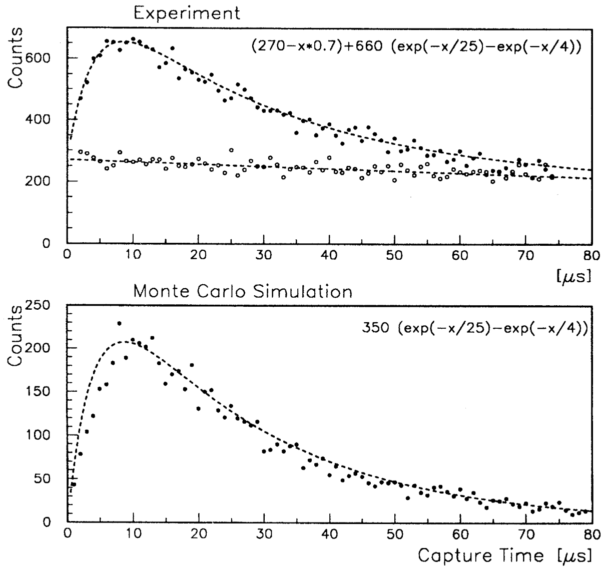

FIG. 5. Above: Measured neutron thermalization and capture time spectrum in a 0.09% Gd-loaded liquid scintillator. The respective time constants are 4 ± 1 μs and 25 ± 3 μs. Below: Monte Carlo calculated neutron thermalization and capture time, in a 0.09% Gd-loaded liquid scintillator. The capture time distribution is in agreement with the experiment.

defined by the fast coincidence of a proton recoil signal ($E > 1$ MeV) in the CUBE and a 4.4-MeV γ signal in a NaI detector, which was placed next to the source-CUBE configuration. By requiring the detection of an energetic recoil signal, only fast neutrons with energies of several MeV were selected. The neutron capture was defined by the detection of the γ cascade ($E_\gamma > 3.2$ MeV). The distribution of the capture times is shown in Fig. 5. The exponential portion of the distribution was fit with a (25 ± 3)-μs decay constant, with a neutron thermalization time of about 4 μs. The observed ratio of 12% between neutron capture signals and fast-coincidence triggers was a measure of the efficiency. This agrees reasonably with the Monte Carlo prediction of about 11%, taking into account the lower energy of the source neutrons and a slightly modified timing cut of 2–76 μs.

E. The different modes of the experiment

The observed neutron-pion excess, N_n is given by the expression,

$$N_n = N_\mu \bar{X} \epsilon Y,$$

where N_μ is the total number of muon triggers, $\bar{X}$ is the average path length of the triggered muons through the CUBE, in units (g/cm^2), ϵ is the neutron-pion detection efficiency, and Y expresses the spallation probability or yield in terms of neutrons and pions produced per (muon g/cm^2) of material traversed. Y is the quantity to be determined in this experiment; it is a function of the average muon energy, and thus of the depth underground.

The average path length of the triggering muons in the detector was determined with a ray-tracing Monte Carlo calculation assuming a $\cos^2\theta$ angular distribution and taking into account the proper geometry of the experimental setup. Three different trigger modes were studied in the experiment leading to three different path lengths for the muons. One aspect of the measurement was to verify the muon origin of the spallation products in the fiducial volume by obtaining the same production yields per path length, in the different experimental modes. For the CUBE-bottom coincidence trigger, requiring only a trigger coincidence between the CUBE and the bottom muon counter, an average path length of 44 cm was determined by our calculation, corresponding to 38 g/cm^2 of material. For another trigger mode, which required the top counter, bottom counter, and main detector in coincidence, the Monte Carlo calculation found the average path length to be 57 cm, or 49 g/cm^2 of scintillator. A third trigger mode was used to investigate the pion production in the liquid scintillator. One source of background for these events are decay products from stopped muons in the bottom trigger paddle, entering the CUBE detector. These events possess the same energy and time characteristics as the contained pion signal. They can, in principle, be vetoed, as the emerging electrons should also have deposited energy in the paddle in which the muons stopped. As a check, a third muon trigger paddle, 33 × 51 cm^2, was added and placed 10.5 cm beneath the bottom trigger paddle. The geometry of this arrangement ensures that the entire thickness of the 60 × 60 cm^2 bottom trigger paddle would be traversed by any Michel electron originating from this third trigger counter, generating a clear veto signal. For this trigger mode, the average muon path length was calculated to be 49 g/cm^2.

II. DATA ANALYSIS

A. Raw data

Figures 6 and 7 present the raw data, before analysis cuts were applied, showing histogrammed energy distributions of ADC1 and ADC2, the energies of first and second delayed events following a valid muon trigger. The spectra shown here correspond to 18.75 days of data taking in the CUBE-bottom trigger mode. The solid lines correspond to events that were correlated with the real muon triggers. This signal includes the background (dashed lines), which contains accidental events — this accidental background histogram was accumulated by the use of the false trigger and is equivalent to the "singles" spectrum in the CUBE.

Correlated counts following a through-going muon are seen, as evidenced by the excess in the real trigger data versus the false in both ADC spectra. In ADC1 (first delayed signal) the excess extends out to highest energy. This energetic enhancement comes possibly from π^+ production, with the delayed count being the Michel positron. In ADC2, however, the excess stops at channel 700 or about 8 MeV. This indicates the absence of correlated double events of high energy.

Figure 8 displays the time distribution of the first delayed signal. The background timing distribution (dashed line) is flat, as expected with a low accidental probability in the 76-μs window. The real signal (solid line) shows two decay constants. The first one is in agreement with the 2.2-μs lifetime from π^+-μ^+ decay; the second one has the 25-μs capture time for neutrons on Gd. The dotted line includes both

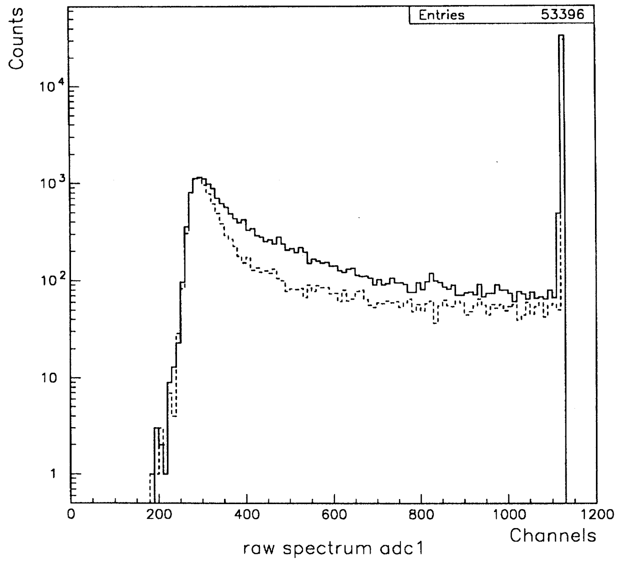

FIG. 6. Energy data from the first delayed event (ADC1) before analysis cuts. The solid histograms are signals correlated with real muon triggers; the dashed lines were data collected by the false triggers. The false spectrum measures the accidental background.

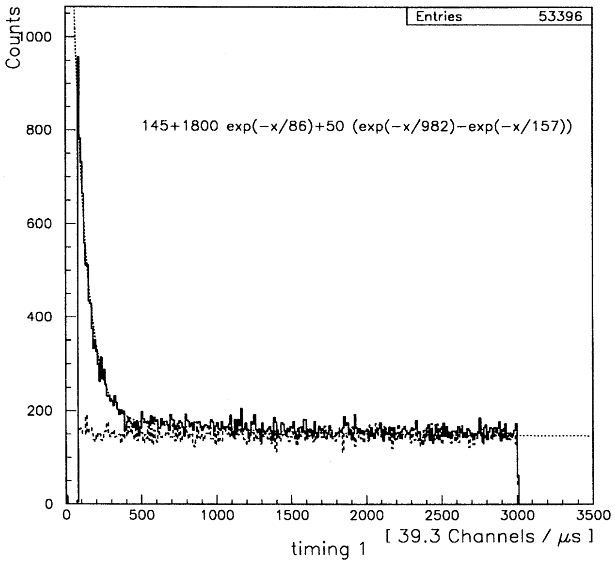

FIG. 8. Timing data from the first delayed event (TAC1) before analysis cuts. The solid histograms are signals correlated with real muon triggers; the dashed lines were data collected by the false triggers. 39.3 channels correspond to 1 μs.

of these exponential decay constants and the 4-μs thermalization time for fast neutrons.

In the subsequent analysis, we placed a time cut on the data, dividing it into two components. For TAC1 values greater than channel 350, equivalent to 9 μs, we attempted to select the neutron component of the correlated counts. For values less than this, we were selecting the 2.2-μs component.

B. Neutrons in the first timing window

Figure 9 shows the ADC1 histograms, after implementing the timing cut (time $>$ 9 μs). To maximize the signal/background ratio, veto cuts have been applied. Only those

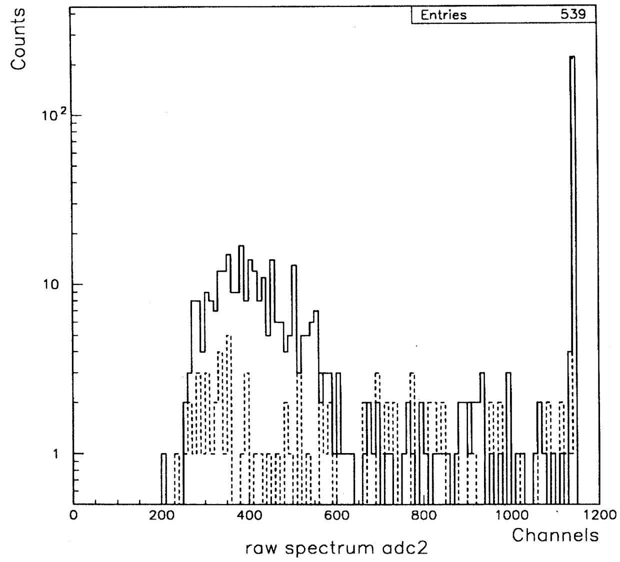

FIG. 7. Energy data from the second delayed event (ADC2) before analysis cuts. The solid histograms are signals correlated with real muon triggers; the dashed lines were data collected by the false triggers. As these events were the second to follow a trigger, the false spectrum measures both the accidental background and correlated first-second count backgrounds.

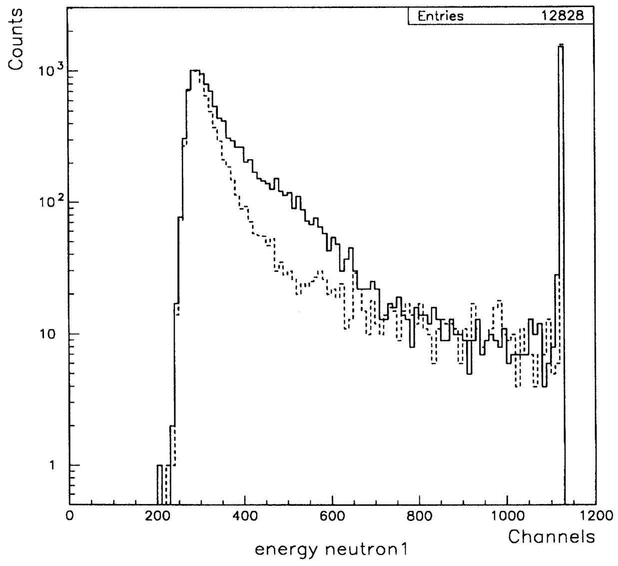

FIG. 9. ADC1 data for muon-induced neutron production. Only events with time >9 μs were selected. Veto cuts from the muon counters were applied to enhance the signal-to-background ratio. The spectrum shows an excess of counts correlated with the through-going muon trigger, in the energy range below 8 MeV. This is as expected for neutron capture on Gd. Above 8 MeV (channel 700) no statistically relevant enhancement is present.

TABLE I. Measured counts and extracted production yields for neutrons and pions. The experimental configuration for each set of runs are designated as *A*, tunnel *A*; *C*, tunnel *C*; c-b, CUBE-bottom trigger; t-b, top-CUBE-bottom trigger; t-b-b, top–CUBE–bottom-1–bottom-2 trigger. All veto, timing and energy cuts described in the text have been taken into account. In runs 495–560, software selection of different trigger modes was possible.

Run	Real counts	False counts	Real-false	Error	N_{trig}	$\bar{X}$ (g/cm^2)	Trigger rate (Hz)	Mode		$\times 10^{-5}$ n / (μ g/cm^2)
Single neutron production										
103–223	11 046	8114	2 932	139	18 500 000	38	11.5	*A*	c-b	3.79±0.18
225–243	10 836	7432	3 404	135	18 640 350	38	11.5	*A*	c-b	4.37±0.18
256–269	4 254	2802	1 452	84	7 200 000	49	6.3	*A*	t-b	3.74±0.22
276–292	4 136	2278	1 858	80	8 500 000	49	6.2	*C*	t-b	4.06±0.18
349–371	2 187	991	1 196	57	4 434 404	49	2.5	*C*	t-b-b	5.00±0.24
400–422	1 214	666	548	44	2 397 100	49	2.7	*C*	t-b-b	4.24±0.34
495–560	10 812	6058	4 754	130	24 095 000	38	11.0	*C*	c-b	4.72±0.13
305–342	3 423	2103	1 320	75	3 606 280	49	1.6	*C*	t-b-b	6.79±0.39
454–479	4 121	2018	2 103	79	8 287 500	38	6.2	*C*	c-b	6.07±0.23
Double neutron production										
103–223	129	8	121	12	18 500 000	38	11.5	*A*	c-b	1.43±0.14
225–243	101	8	93	11	18 640 350	38	11.5	*A*	c-b	1.09±0.13
256–269	55	5	50	8	7 200 000	49	6.3	*A*	t-b	1.18±0.19
276–292	112	7	105	11	8 500 000	49	6.2	*C*	t-b	2.10±0.22
349–371	66	2	64	9	4 434 404	49	2.5	*C*	t-b-b	2.45±0.35
400–422	37	0	37	6	2 397 100	49	2.7	*C*	t-b-b	2.62±0.42
495–560	191	5	186	14	24 095 000	38	11.0	*C*	c-b	1.69±0.13
305–342	71	3	68	9	3 606 280	49	1.6	*C*	t-b-b	3.26±0.42
454–479	108	2	106	11	8 287 500	38	6.2	*C*	c-b	2.80±0.29
π^+ production										
256–269	860	135	725	32	7 200 000	49	6.3	*A*	t-b	0.342±0.015
276–292	1 001	179	822	34	8 500 000	49	6.2	*C*	t-b	0.329±0.014
349–371	614	100	514	27	4 434 404	49	2.5	*C*	t-b-b	0.394±0.021
400–422	326	61	265	20	2 397 100	49	2.7	*C*	t-b-b	0.376±0.028
495–560	754	91	663	30	6 336 985	49	2.9	*C*	t-b-b	0.356±0.016
305–342	724	116	608	29	3 606 280	49	1.6	*C*	t-b-b	0.573±0.028
π^+-n production										
256–269	70	0	70	9	7 200 000	49	6.3	*A*	t-b	0.301±0.038
276–292	77	0	77	9	8 500 000	49	6.2	*C*	t-b	0.280±0.033
349–371	50	2	48	7	4 434 404	49	2.5	*C*	t-b-b	0.335±0.049
400–422	35	0	35	6	2 397 100	49	2.7	*C*	t-b-b	0.451±0.077
495–560	82	0	82	9	6 336 985	49	2.9	*C*	t-b-b	0.400±0.044
305–342	76	0	76	9	3 606 280	49	1.6	*C*	t-b-b	0.652±0.077

events not accompanied by a muonlike energy deposit in any one of the muon veto paddles were selected. Correlated events manifest themselves as excess counts over the background; the excess stops at channel 700, roughly 8 MeV. Above channel 700, no statistically significant excess is present, including the overflow bin. The time distribution of these events agrees with the expected single-component exponential of 25 μs. The neutron origin of these selected correlated events is confirmed.

The possible correlated backgrounds to the single-neutron signal come from external neutron production. These might be neutrons produced from the capture of μ^-, either in the bottom veto paddle or from the ground underneath the detector. Another source would be spallation neutrons produced outside of the detector by the muon, which ultimately passed through the CUBE, triggering the electronics. These rates can be estimated using our knowledge of the production of neutrons by muon capture [7] and spallation. Considering that the detector is situated 76 cm above the floor, providing for a small opening angle for neutrons produced in the ground to reach the detector, we find that these background rates are negligible.

Table I and Fig. 10 summarize the production yield of single neutron events, for the different experimental configurations used in the different runs of the experiment. The mean value for the single neutron production yield is

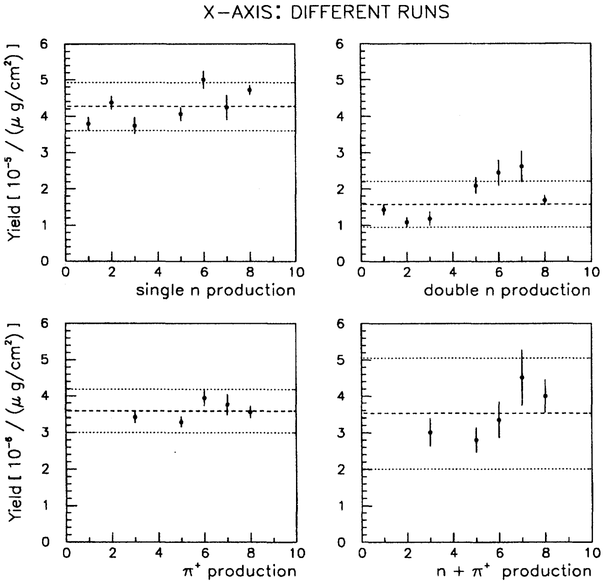

FIG. 10. The production yields for single-neutron, double-neutron, π^+ and π^+-n production in different experimental modes. Runs 1–3 were performed in tunnel A of the Stanford Underground Facility, runs 5–8 in tunnel C. The trigger mode for runs 1, 2, and 8 was CUBE–bottom-1 coincidence, for runs 3 and 5 it was top–CUBE–bottom-1 and for runs 6 and 7 it was top–CUBE–bottom-1-bottom-2. The difference in the average muon path length between the modes has been accounted for and does not influence the measured production yields. All veto, timing and energy cuts described in the text have been taken into account. The dashed lines correspond to the mean values of all respective subexperiments; the dotted lines show the statistical 3 σ error range.

$(4.3 \pm 0.3 \pm 0.8) \times 10^{-5}[1n/(\mu \text{ g/cm}^2)]$. This result contains the dominating systematic error of 20% from the neutron detection efficiency.

C. The π^+ signal

The pion efficiency of our detector is governed by the escape probability of the pions, the probability of the decay positrons to deposit energy in the CUBE above the threshold, and the software timing and veto cuts. Based on the ≈ 5-cm range of 100-MeV pions, a geometrical ray-tracing calculation finds a 10% escape probability. For the Michel positrons, an EGS4 Monte Carlo simulation estimates a detection efficiency of 95%, for deposited energy greater than 3.2 MeV. Selecting signals between 0.5 and 9 μs as pion decay events gives an efficiency of 78%. We include a 90% efficiency term to account for the self-vetoing of the pion events spilling out of the detector into the muon veto counters. These come mostly from Michel e^+ produced close to the edges of the detector, where energy could have been deposited in the adjacent veto counters, rejecting the event. Thus, the overall detection efficiency for the pion events is estimated to be 60%, with a relative error of 20%.

Several sources of background can contribute to pionlike signals occurring within the first 9 μs. One source comes from muons stopping in the lower muon trigger paddle. Though stopped, these muons could still have triggered the data acquisition. The energetic μ-decay electrons have a sizable range in plastic (≈10 cm) and some fraction of them could have penetrated into the CUBE, depositing delayed, correlated energy greater than 3.2 MeV with the correct timing behavior.

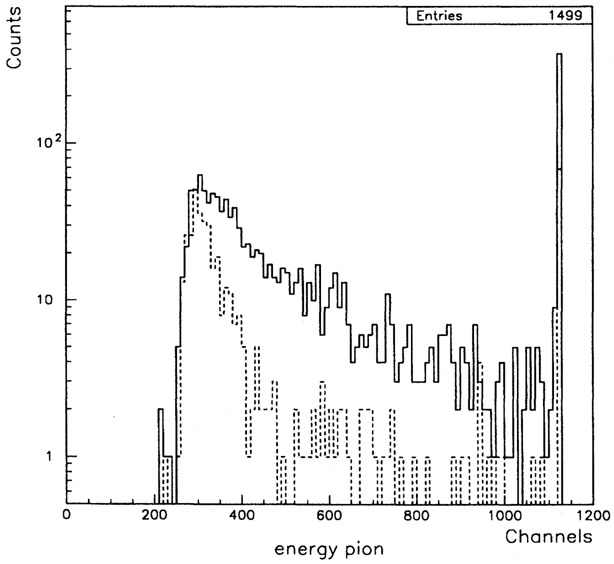

FIG. 11. ADC1 data for muon-induced pion candidates. Only events with time <9 μs were selected. Veto cuts from the muon counters were applied. The spectrum shows an excess of counts correlated with the through-going muon trigger over the whole energy range. To determine the π^+ production yield, only data above 8 MeV (channel 700) were considered to eliminate the contribution from neutrons.

We seek to reject them by looking for their energy loss as they emerged from the bottom muon counter. Some of these $e^\pm$ might have passed through only a small amount of material in the veto paddle. When taking data in modes with only one bottom-trigger paddle, a restrictive veto cut just above the ADC pedestal had to be applied to suppress these background events. As described previously, a second bottom-trigger paddle was installed for some portion of the data collection, in which the decay $e^\pm$ from muons, which stopped in this counter, had to penetrate the first paddle, directly below the CUBE, in order to be recorded as a delayed event in the detector. A cross check that this was effectively rejecting the stopped muon background was performed.

Another potential source of background was the decay of upward-scattered muons, which stopped in the CUBE and triggered the data acquisition. The purpose of including a top-trigger counter in some runs was to eliminate these events. In any case, a comparison between the two trigger modes (CUBE-bottom and top-CUBE-bottom) showed this background to be small.

Neutrons can be eliminated from the pion data set by selecting only those events that deposited more than 8 MeV (in addition to the time cut <9 μs). To account for the neglected counts at lower energy, one can scale the missing fraction using the contents of the spectra above 8 MeV and below the overflow bin of the ADC. An EGS4 Monte Carlo simulation was employed to correct for the missing counts, finding a factor of 1.125 for acceptance of positrons down to 3.2 MeV.

Figure 11 displays the total energy range in ADC1 of the selected pionlike signals. The spectrum contains neutron and pion signals only; the veto cuts described above, were included. Without these cuts the contents of the spectra would have been 7338 and 1879 counts (real and false, respectively). With the veto cuts, the contents are 1499 and 435 (illustrating the rejection of the stopped muon-decay background). A large signal over background excess is present and extends over the whole spectrum, as expected for the broad energy distribution of the μ-decay positrons. When selecting only those events with an energy deposit larger than 8 MeV, the time distribution of the correlated events shows a single exponential decay constant in agreement with 2.2 μs.

Table I and Fig. 10 provide a survey of the production yield of π^+ events. Unlike the neutron evaluation, the first two runs do not contribute in this table, as these data were taken with the CUBE-bottom trigger mode and did not include the top trigger. The analysis of run 8 (495–560 in Table I) was performed with the inclusion of a top-paddle trigger off line. The mean value of the distribution is $(3.5\pm0.2\pm0.7)\times10^{-6}[\pi^+/\ (\mu\ \mathrm{g/cm}^2)]$, including the dominating systematic error of 20% from the detector efficiency.

D. Double neutrons

In this section we focus on events in which two neutron capture candidates were recorded following a muon trigger. Similar selection cuts can be employed to extract the double-neutron production yield from the data as for the single neutrons. However, the background collected with the false trigger must be reevaluated when considering events that contain two delayed counts. For the single-neutron and pion data, real muon-triggered events contain data that might be time correlated with the initial muon trigger; false events refer to data that were purely accidental. However, in events with two delayed counts, it could be that the second count was correlated with the muon, the first event, or that the second count occurred purely accidentally.

Several background sources can create correlated first-second event signatures. An example is an accidental stopped muon following the original muon trigger within the first 76 μs. The stopped muon would be detected as the first delayed count and its decay electron as the second delayed event. Alternatively, an accidental muon in the first timing window could create a neutron via spallation in the CUBE, and the subsequent capture of the neutron might be detected in the second window. These are background processes that have a purely accidental first event. Consequently, the occurrence of these events within the first timing window should be equally probable under the real or false trigger.

Thus, in comparison to the single-neutron analysis, the accidental background in the second timing window is not trivially extracted by using the false trigger counting. Furthermore, the number of times the second timing window was opened differs between real and false events — the second window was opened only when a first delayed event was observed. Since we observed real neutron and pion correlated events in excess, the real first event rate was larger than the false first event rate. The accidental background counts for the second events in the real data set had to be scaled up from the false trigger data.

All of these corrections were properly taken into account. However, as the backgrounds for the production of double neutrons or π^+-n events were very small, their minimal contributions led only to minor corrections in the counting analysis.

For the selection of a double-neutron event, we required that a first neutron was already detected under application of all the veto, timing, and energy cuts described previously. For the second neutronlike signal, we required the same veto and energy cuts as were applied for the single neutron. No additional timing cut was necessary in the second time window, as the first timing cut ($>9\ \mu$s) was sufficient to reject the pions from the data sample and to allow both neutrons to thermalize.

Considering the detection efficiency for double neutrons, we return to the problem of their energy spectrum. Since two neutrons share the excitation energy, it seems reasonable that, per neutron, the energy would be lower than in single-neutron emission. However, the mechanism to produce double neutrons via π^- capture on a pseudodeuteron would instead suggest a broader and flatter spectrum; neutron spectrum measurements by Madey *et al.* [8] seem to concur. As an approximation, we applied the same 37% effective neutron capture probability on both neutrons (0.37^2); thus we were assuming that each neutron would have the same capture probability as if they were emitted individually. The detection of both cascades of neutron capture γ's firing the 3.2 MeV threshold contributes with 0.38^2 to the efficiency.

Last, the capture time distribution of the first neutron is affected by the presence of the second neutron. As the first capture could have been from either neutron, the probability of observing the first interaction is doubled; the mean capture time constant is reduced to half of its normal value. Taking into account this shortened capture time of 12.5 μs, we find an acceptance of 60% for the first time window (9–76 μs). In the second window, the normal 25 μs capture time applies, and we have only to account for the 0.5 μs of hardware deadtime (no additional timing cut was applied). Thus, we arrive at a total efficiency for the detection of double-neutron events of $(1.2\pm0.4)\%$.

Table I and Fig. 10 summarize the production yield of double neutron events, for the different experimental configurations used in the different runs of the experiment. The mean value for the double-neutron production yield is $(1.6\pm0.2\pm0.5)\times10^{-5}[2n/(\mu\ \mathrm{g/cm}^2)]$, including the dominating systematic error of 30% from the detection efficiency.

E. Associated pion-neutron production

For neutrons that are released in violent muon-induced nuclear disintegrations, it is possible that free pions are produced in the resultant high-energy hadronic showers or cascades. Thus, neutrons could be accompanied by pions. Alternatively, lower-energy interactions might lead to neutron production that actually proceed via pion intermediaries. That is, the secondary pion-nuclear interactions might contribute significantly to the production of fast neutrons.

In searching for correlated π^+-n pairs, one expects to detect the π^+ event first, because of its short decay time. Following this, we applied all the veto, timing, and energy cuts for the detection of the π^+ as a first signal. In addition, we imposed the same energy and veto cuts as in the above analysis for the second neutron and required a timing cut for the neutron detection of at least 9 μs $-$ TAC1, where TAC1 was the time of the π^+ event. This was necessary, since the pion is usually detected much before the thermalization of the neutron. Using these cuts, the efficiency for the detection of such an event is given by the product of the efficiency for the π^+ detection and the efficiency for single-neutron detection: $\epsilon = 0.60 \times 0.11 = 0.066$.

For the background subtraction, the same procedure as for the double neutrons could be used to scale the accidental false rate. Because of the small background rate in the first timing window for the π^+, the accidental background rate in the second window was close to zero. Thus, all background that was observed in the second false spectrum was attributed to background counts of the correlated first-second nature.

Table I and Fig. 10 summarize the production yield of π^+-n pairs, for the different experimental configurations used in the different runs of the experiment. Unlike the neutron evaluation, the first two runs do not contribute in this table, as these data were taken with the CUBE-bottom trigger mode, without including the top trigger. The analysis of run 8 was performed with the inclusion of a top-paddle trigger off line. The mean value for the production yield of π^+-n is $(3.5\pm0.2\pm1.0)\times10^{-6}[\pi^+\text{-}n/(\mu\ \text{g/cm}^2)]$. In this result, the dominating systematic error of 30% from the detector efficiency is included.

The yield of π^+-n events is the same as the production yield extracted for π^+ alone, after correcting for detection efficiency. Thus, we conclude that almost all of the pions produced by muon-nuclear inelastic interactions are accompanied by one or more neutrons.

F. Dependence on the trigger energy of the muon

Cosmic-ray muons are able to produce hadronic or electromagnetic cascades. If a muon produces a cascade in the concrete of the lab or in the detector, the shower will approximately follow the incident direction of the muon, with particles possibly entering the CUBE and/or the muon trigger paddles.

A trigger by a shower should therefore release a high signal in several muon counters. We installed, as the last submeasurement in this experiment, an additional ADC recording the energy deposited by the triggering muon in the respective paddles. Off line, we were able to place cuts on the energy deposited in the trigger paddles. In this data-taking mode (see Table I, runs 495–560 and Fig. 10, run 8), we maintained the most general hardware trigger mode, requiring that the CUBE and the first bottom paddle should fire the data acquisition. All other trigger modes were simulated by using the information readout from the muon-trigger ADC's.

The background subtraction technique with the false trigger had to be modified in this mode as there was no information available on the muon hit distribution. To correct for this, a measurement with high statistics of the muon triggering rates, as a function of the trigger modes, and a measurement of the trigger energies allowed a determination of the scaling factors to be used for accidental background subtraction, based upon the measured CUBE-bottom trigger false spectra. This is the correct procedure for signals falling in the first timing window, but is no longer strictly correct for the signals from the second window. Fortunately, these data were virtually free of background such that the minor background scaling error was unimportant.

To check the validity of this method, two further tests were performed using modified muon hardware thresholds, so that the false background could be precisely extracted. In these measurements, the trigger thresholds for the first and second bottom paddle were increased (separately in two runs) such that the trigger rate in both cases dropped by a factor of 2 (see Table I, runs 305–342 and 454–479). The trigger modes employed were the CUBE–bottom-1 and the top–CUBE–bottom-1–bottom-2 hardware coincidences. Examining these data showed that both the hardware-modified trigger-threshold case and the software analyzed method were in agreement.

Searching for correlated high-energy deposits in several muon paddles should allow the selection of showering events. We investigated the muon trigger data, finding the fraction of signals in the overflow channel for the top paddle, the bottom-1 paddle and the bottom-2 paddle to be 9.4%, 5.4%, and 0.84% of the total spectra, respectively. Searching for coincident overflow signals in the top and the bottom-1 paddle, or in all three counters, we found the fraction of events, which possessed coincident high-energy signals, to be 0.78% and 0.2%, respectively. If this were due solely to chance occurrence of energy deposition large enough to be in the overflow for each counter, one would expect 0.5% and 4×10^{-5}; it is likely that these events were correctly attributed to showering muons (hadronic or electromagnetic).

The enhancement of the production yield of neutrons and pions by the showering muon events was investigated. Energy cuts were placed simultaneously in the top, bottom-1, and bottom-2 paddle (when applicable). These results are displayed in the left half of Fig. 12. The x axes of the plots show where the energy cut was placed (i.e., 500 means that only those trigger events depositing more energy than channel 500, simultaneously in all triggering counters, were selected). The yields were normalized per muon-triggered event, demonstrating that showering events are much more efficient (up to a factor of 100 enhancement) in producing neutrons or pions.

An interesting result appears, looking at the comparison between second $(2n,\pi^+n)$ and first $(1n,1\pi^+)$ events. By selecting a high energy threshold for the muon shower, the yields for $1n(1\pi^+)$ and $2n(\pi^+n)$ production become similar. This indicates that we were indeed detecting events in which multiple hadronic particles were present in the CUBE, and it is a strong indication that we were selecting the hadronic showers accompanying the muon.

Displayed on the right half of Fig. 12 is the converse situation to the previous, where we placed the energy cuts simultaneously in the top, bottom-1 and bottom-2 paddle to exclude the high-energy part of the muon spectra. The x axes of the plots show where the energy cut was placed (i.e., 500 means that only those trigger events depositing less energy than channel 500 in the muon-trigger counters but more energy than required for a minimum-ionizing muon, were included). We would expect to measure a constant yield, independent of the muon energy deposition, once the contribution from showering muons were excluded by the cuts. In this figure, an approximately constant behavior appears. The residual dependence of the production yield on the value of the muon energy is caused by two nonidealities: not all showers will produce the maximum energy deposit in all trigger paddles, such that some showering muon events are present in this data sample; second, in the calculation for the yield, we used the same average muon path length for all values of the muon energy cut. Strictly speaking, this would not be correct, as the energy deposited in the triggering counters depends on the angle of incidence of the muon, and by applying the energy cuts we were selecting slightly varying path lengths in the CUBE.

We attribute the average value of the yields from Fig. 12 to the contribution of muons alone to the production yield of neutrons and pions. The single-neutron production drops to $2\times10^{-5}[1n/(\mu\ \mathrm{g/cm^2})]$, the double-neutron production becomes $0.5\times10^{-5}[2n/(\mu\ \mathrm{g/cm^2})]$, the π^+ production becomes $2.5\times10^{-6}[\pi^+/(\mu\ \mathrm{g/cm^2})]$, and the π^+-n production falls to $1\times10^{-6}[\pi^+\text{-}n/(\mu\ \mathrm{g/cm^2})]$ in these non-showering muon-induced events. We observed that the ratio between single- and double-neutron production in nonshowering events increases from 2.7 to roughly 4:1 and that the ratio of pion events to pions accompanied by neutrons increases from 1:1 to about 2.5:1, in the nonshowering case.

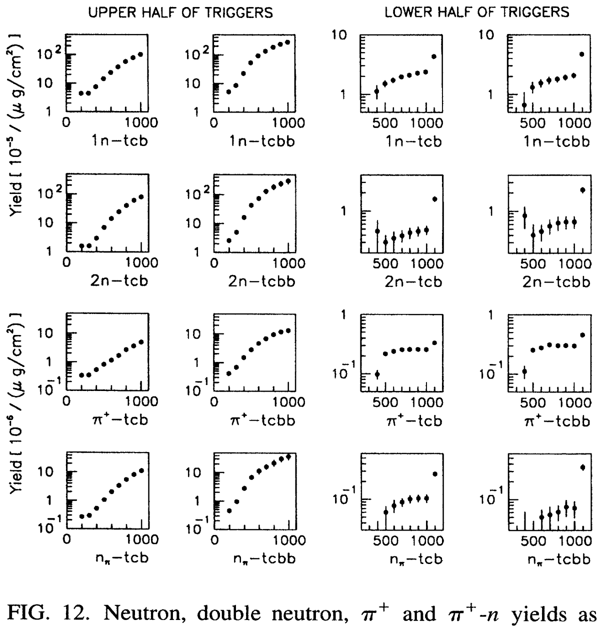

FIG. 12. Neutron, double neutron, π^+ and π^+-n yields as a function of the energy threshold used for the muon triggers. In the left two columns, selection of the upper part of the muon spectrum was examined. In the right plots of the figure, only the lower part of the trigger spectrum was included. The x axis gives the lower or upper cut applied in the respective situations.

III. DISCUSSION

A. Relating neutrons and pions

From the nonshower production yield of π^+ events we can estimate the amount of double-neutron production via π^- capture on pseudodeuterons in carbon. Under the assumption that π^+ and π^- creation are equally likely in the muon-nucleus interaction, one would obtain a rate of $2.5\times10^{-6}[2n/(\mu\ \mathrm{g/cm^2})]$, which is about half of the observed double-neutron production yield from nonshowering muons. Thus, a large fraction of the double-neutron events proceed via pion intermediaries, even in the case of nonshowering muon-nuclear interactions. Nevertheless, multiple neutrons created in hadronic showers are, even at this shallow depth, about twice as frequent as multiple neutrons from nonshowering events.

Summing the neutron production yields from all associated pion channels, including the above estimate of the π^--capture neutron rate, one finds that neutrons accompanying pions constitute half the measured rate of neutron production by nonshowering muons. Here, we assume that all pion isospins are equally produced by muon spallation and that the probability for adjoint neutron emission is the same in each reaction. Since the energy release is fairly high in muon interactions, which produce pions, this assumption might be acceptable, despite the fact that only π^+ production leads directly to a neutron-rich final state (^{12}B nucleus). This result strengthens the conclusion that pion intermediaries play a large role in the muon-induced production of neutrons.

B. Comparison to other experiments

A similar experiment has been performed by Bezrukov *et al.* [9] at a 25-mwe depth. The main difference between our experiment and this other shallow depth experiment was the use of several tons of passive paraffin shielding surrounding their detector. The presence of material so close to the

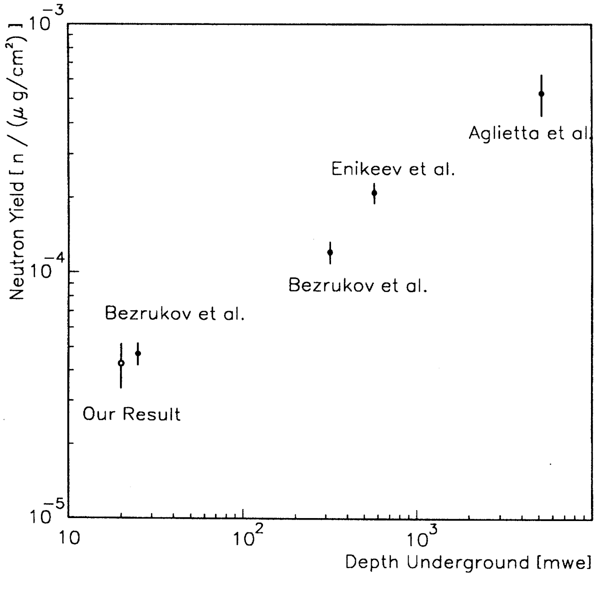

FIG. 13. World plot of underground neutron yield measurements.

neutron-sensitive volume makes it more difficult to investigate events involving multiple particles, as detection efficiency becomes strongly dependent on the position where the multiple hadronic events were produced. Secondary production of hadrons, showering in the paraffin, becomes probable. Reference [9] observed double-neutron events but did not give results concerning the production yield of double neutrons by muons. In addition, pion and pion-neutron production were not accessible in this experiment.

Bezrukov *et al.* [9] quote a neutron spallation yield of $(4.7\pm0.5)\times10^{-5}$ neutrons per muon g/cm^2, which has to be compared to our value of $(4.3\pm0.3\pm0.8)\times10^{-5}$ neutrons per muon g/cm^2, at 20 mwe. As the average muon energy increases with depth underground, so does the neutron spallation yield. This depth dependence is given in Ref. [10], as well as a comparison of the results of neutron yield measurements from the four experiments that have been performed so far [9–11]. These results, at four different depths, and our measured neutron yield at 20 mwe, are plotted in Fig. 13. Our data point shows good agreement with the general trend of neutron yield versus underground depth, as displayed in this world plot.

C. Conclusions

The motivation for this experiment, which measured the neutron yield and multiplicity following muon spallation, was to further our understanding of the neutron backgrounds at shallow depths. Despite the fact that the general features of the muon spallation process have been known since the early 1950's, a complete understanding of the exact nature of all aspects of the production of fast neutrons has not been reported. In examining the production mechanisms for hadrons, we were particularly interested in studying pion production and the production of double neutrons and pion-neutron pairs, aspects previously not explored.

In this experiment, we measured the spallation yields on a liquid scintillator target (carbon), at an underground depth of 20 mwe. The experiment was strongly motivated by background studies for the San Onofre reactor neutrino oscillation experiment. Our result for neutron production of $(4.3\pm0.3\pm0.8)\times10^{-5}$ neutrons per muon g/cm^2 agrees with other experimental measurements of underground neutron production by cosmic-ray muons. This yield implies that the San Onofre experiment is most likely not limited by fast spallation neutrons from muons.

Hadron production by inelastic scattering of muons occurs for both showering and nonshowering interactions. This measurement attempted to disentangle both situations by examining the energy deposited by muons and/or showers in the triggering counters. For the showering case, the production of neutrons and pions in the detector was observed to become orders of magnitude more efficient than for nonshowering muons. Despite the fact that at 20 mwe the number of muons creating showers (in particular, hadronic cascades) amounts only to a few percent of all muons, the nonshowering production yield compared to the general neutron production yield decreases by only a factor of 2, to 2×10^{-5} neutrons per muon g/cm^2. Similarly, for double-neutron, π^+, and π^+-n production, we observed decreased production yields, by factors of 3.2, 1.4, and 3.5, respectively, when only nonshowering muons were selected.

From our observation of $\pi^+\rightarrow\mu^+\rightarrow e^+$ events, we determined that pions contribute substantially to the production of neutrons by muons. Additionally, the observation of associated pion-neutron production confirms that a large fraction of the produced pions are accompanied by neutrons, either created simultaneously in hadronic cascades or coming from neutron production via secondary pion reactions. The results of this measurement have been compared to the calculation of Delorme *et al.* [12] and proved essential in testing their method of equivalent photons for the study of pion production by muons.

ACKNOWLEDGMENTS

We would like to thank Professor F. Boehm and Professor B. Cabrera for supporting this work. Discussions with P. Vogel, T.E.O. Ericson, M. Ericson, and O.G. Ryazhskaya were invaluable and are gratefully acknowledged. We are also greatly indebted to B. Chugg for his assistance during the data taking period. One of the authors (R.H.) would like to thank the Alexander von Humboldt Foundation for financial support. This research was supported by the U.S. DOE under Grant Nos. DE-FG03-88ER40397 and DE-FG03-90ER40569.

---

[1] F. Boehm *et al.*, Proposal for the San Onofre Neutrino Oscillation Experiment, California Institute of Technology, 1994; M. Chen *et al.*, Nucl. Phys. **BS35**, 447 (1994).
[2] A. da Silva *et al.*, Nucl. Instrum. Methods A **354**, 553 (1995).
[3] J.C. Barton, *Proceedings of the 19th International Conference on Cosmic Rays*, La Jolla, 1985, Physical Society, London (Institute of Physics, London, 1985), p. 98.
[4] O.G. Ryazhskaya (private communication).
[5] M. Chen, V.M. Novikov, and B.L. Dougherty, Nucl. Instrum. Methods A **336**, 232 (1993).
[6] Nucl. Data Sheets **56**, 2 (1989).
[7] S. Charalambus, Nucl. Phys. **A166**, 145 (1971).
[8] R. Madey *et al.*, Phys. Rev. C **25**, 3050 (1982).
[9] L.B. Bezrukov *et al.*, Sov. J. Nucl. Phys. **17**, 51 (1973).
[10] M. Aglietta *et al.*, Nuovo Cimento C **12**, 467 (1989).
[11] R.I. Enikeev *et al.*, Sov. J. Nucl. Phys. **46**, 1492 (1987).
[12] J. Delorme *et al.*, Phys. Rev. D (submitted).

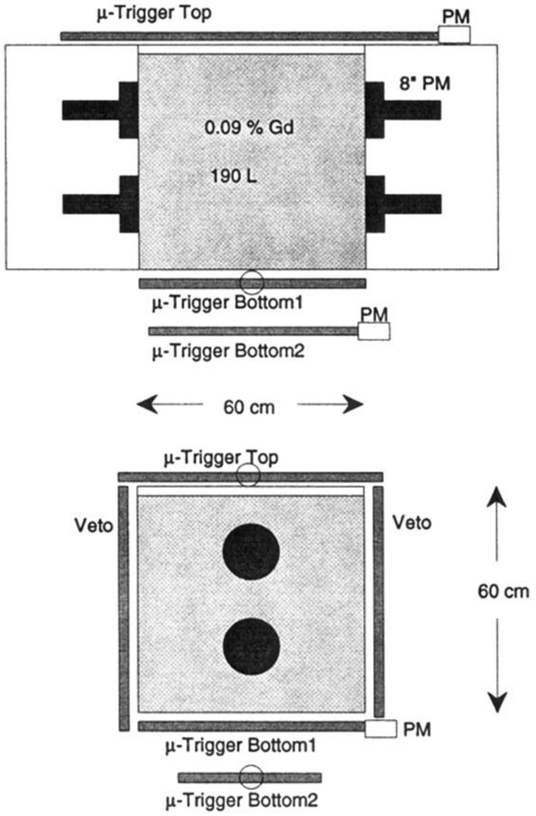

FIG. 1. The CUBE detector with muon veto counters. The top and the bottom veto paddles also served as trigger counters.

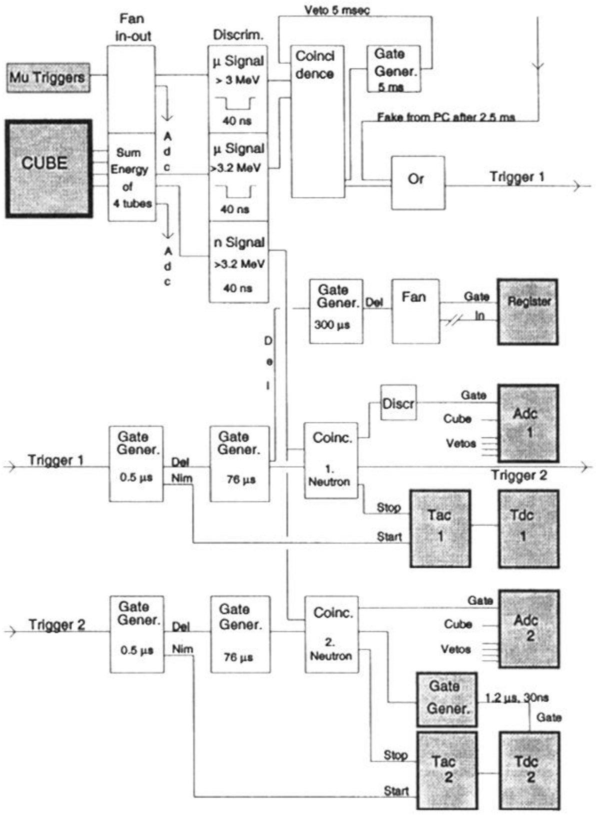

FIG. 2. Schematic of the CUBE electronics. The shaded items to the left were detector components; shaded items to the right were CAMAC modules; unshaded modules were implemented in NIM crates.